

Collective excitations on a surface of topological insulator

D. K. Efimkin¹, Yu. E. Lozovik^{1,2,*} and A. A. Sokolik¹

¹*Institute for Spectroscopy RAS, 142190, Troitsk, Moscow Region, Russia*

²*Moscow Institute of Physics and Technology, 141700, Moscow, Russia*

We study collective excitations in a helical electron liquid on a surface of three-dimensional topological insulator. Electron in helical liquid obeys Dirac-like equation for massless particles and direction of its spin is strictly determined by its momentum. Due to this spin-momentum locking, collective excitations in the system manifest themselves as coupled charge- and spin-density waves. We develop quantum field-theoretical description of spin-plasmons in helical liquid and study their properties and internal structure. Value of spin polarization arising in the system with excited spin-plasmons is calculated. We also consider the scattering of spin-plasmons on magnetic and non-magnetic impurities and external potentials, and show that the scattering occurs mainly into two side lobes. Analogies with Dirac electron gas in graphene are discussed.

PACS numbers: 73.20.Mf, 73.22.Lp, 75.25.Dk

I. INTRODUCTION

Topological insulator is a new class of solids with non-trivial topology, intrinsic to its band structure. Theoretical and experimental studies of topological insulators grow very rapidly in recent years (see [1, 2] and references therein). Three-dimensional topological insulators are insulating in the bulk, but have gapless surface states with numerous unusual properties. These states are topologically protected against time-reversal invariant disorder. When gap is opened in surface states by time-reversal or gauge symmetry breaking, a spectacular magnetoelectric effect arises [3, 4].

Recently a “new generation” of three-dimensional topological insulators (the binary compounds Bi_2Se_3 , Bi_2Te_3 and other materials), retaining topologically protected behavior at room temperatures, were predicted and studied experimentally [5–7]. Band structure of the surface states of these materials contain a single Dirac cone, where electrons obey two-dimensional Dirac equation for massless particles. Direction of electron spin in these states is strictly determined by their momentum, so these states can be called as “helical” ones. Surface of topological insulator can be chemically doped, forming charged helical liquid. The spin-momentum locking leads to interesting transport phenomena including coupled diffusion of spin and charge [8], inverse galvanomagnetic effect (generation of spin polarization by electric current) [9] and giant spin rotation on an interface between normal metal and topological insulator [10]. The spin-momentum locking offers numerical opportunities for various spintronic applications.

Collective excitations (plasmons) in helical liquid on the surface of topological insulator was considered in [11]. It was shown that due to spin-momentum locking responses of charge and spin densities to external electromagnetic field are coupled to each other. There-

fore the plasmons in the system should manifest themselves as coupled charge- and spin-density waves and can be called “spin-plasmons”. In [12] application of spin-plasmons in spin accumulator device was proposed. Also surface plasmon-polaritons under conditions of topological magnetoelectric effect were considered in [13].

Properties of the states on a surface of three-dimensional topological insulator are similar to those of electrons in graphene. Graphene is unique two-dimensional carbon material with extraordinary electronic properties [14–16]. Its band structure contains two Dirac cones with electrons behaving as massless Dirac particles in their vicinities. Graphene is a perspective material for nanoelectronics due to large carrier mobilities at room temperature. Electronic interactions and collective excitations in graphene have been extensively studied (see [17] and references therein). In particular, the properties of plasmons [18, 19] and hybrid plasmon-photon [20] and plasmon-phonon [21, 22] modes were investigated theoretically and experimentally. It was realized recently that graphene is a fertile ground for quantum plasmonics [23] due to very small plasmon damping.

In this article, we develop quantum field-theoretical formalism to describe plasmons in graphene and spin-plasmons on a surface of three-dimensional topological insulator based on random phase approximation. Problems of excitation, manipulation, scattering and detection of single plasmons can be conveniently considered using this approach. Thus, this approach can be especially useful for problems of plasmon quantum optics and quantum plasmonics. We use our approach to study internal structure and properties of spin-plasmons in a helical liquid.

The rest of this paper is organized as follows. In section 2, we present a brief description of electronic states on a surface of topological insulator and in graphene. In section 3, quantum field-theoretical description of plasmons in Dirac electron gas is given. In section 4, we consider internal structure of plasmons. In section 5, different consequences of spin-momentum locking are considered. Scattering of plasmons on impurities and external poten-

* lozovik@isan.troitsk.ru

tials is considered in section 6, and section 7 is devoted to conclusions.

II. DIRAC ELECTRONS

The low-energy effective Hamiltonians for electrons in helical liquid [24] and graphene [16] are

$$\text{helical liquid: } H_0 = v_F(p_x \sigma_y - p_y \sigma_x), \quad (1)$$

$$\text{graphene: } H_0 = v_F(p_x \sigma_x + p_y \sigma_y), \quad (2)$$

where the Fermi velocities of electrons v_F are $6.2 \times 10^5 \text{ m/s}$ for the topological insulator Bi_2Se_3 and 10^6 m/s for graphene; the Pauli matrices σ_x and σ_y act in the spaces of electron spin projections (helical liquid) or sublattices (graphene). The eigenfunctions of (1)–(2) can be written as $e^{i\mathbf{p} \cdot \mathbf{r}} |f_{\mathbf{p}\gamma}\rangle / \sqrt{S}$, where S is the system area and $|f_{\mathbf{p}\gamma}\rangle$ is the spinor part of the eigenfunction, corresponding to electron with momentum \mathbf{p} from conduction ($\gamma = +1$) or valence ($\gamma = -1$) band:

$$\text{helical liquid: } |f_{\mathbf{p}\gamma}\rangle = \frac{1}{\sqrt{2}} \begin{pmatrix} e^{-i\varphi_{\mathbf{p}}/2} \\ i\gamma e^{i\varphi_{\mathbf{p}}/2} \end{pmatrix}, \quad (3)$$

$$\text{graphene: } |f_{\mathbf{p}\gamma}\rangle = \frac{1}{\sqrt{2}} \begin{pmatrix} e^{-i\varphi_{\mathbf{p}}/2} \\ \gamma e^{i\varphi_{\mathbf{p}}/2} \end{pmatrix} \quad (4)$$

(here and below we assume $\hbar = 1$). Another difference between helical liquid on a surface of topological insulator and electron liquid in graphene is additional fourfold degeneracy $g = 4$ of electronic states in graphene by two spin projections and two nonequivalent valleys.

The value of electron spin in helical liquid and of pseudospin graphene in the state $|f_{\mathbf{p}\gamma}\rangle$ is

$$\text{helical liquid: } \langle f_{\mathbf{p}\gamma} | \boldsymbol{\sigma} | f_{\mathbf{p}\gamma} \rangle = \gamma [\hat{\mathbf{z}} \times \hat{\mathbf{p}}], \quad (5)$$

$$\text{graphene: } \langle f_{\mathbf{p}\gamma} | \boldsymbol{\sigma} | f_{\mathbf{p}\gamma} \rangle = \gamma \hat{\mathbf{p}}, \quad (6)$$

where $\hat{\mathbf{p}}$ and $\hat{\mathbf{z}}$ are unit vectors directed along the momentum \mathbf{p} and the z -axis respectively. We see that, in helical liquid, the spin of electron lies in the system plane and makes an angle 90° (in counterclockwise direction in the conduction band and inversely in the valence band) with its momentum. In graphene, the sublattice pseudospin of electron is directed along its momentum in conduction band and opposite to it in the valence band. Physically, a definite direction of the pseudospin in the system plane corresponds to definite phase shift between electron wave functions on different sublattices.

A starting point for quantum field-theoretical consideration of plasmons on the surface of topological insulator and in graphene is the many-body Hamiltonian of electrons with Coulomb interaction between them:

$$\begin{aligned} H = & \sum_{\mathbf{p}\gamma} \xi_{p\gamma} a_{\mathbf{p}\gamma}^+ a_{\mathbf{p}\gamma} + \frac{1}{2S} \sum_{\mathbf{q}\mathbf{p}\mathbf{p}'} \sum_{\gamma_1\gamma_2} \sum_{\gamma'_1\gamma'_2} V_{\mathbf{q}} \\ & \times \langle f_{\mathbf{p}+\mathbf{q},\gamma'_1} | f_{\mathbf{p}\gamma_1} \rangle \langle f_{\mathbf{p}'-\mathbf{q},\gamma'_2} | f_{\mathbf{p}'\gamma_2} \rangle \\ & \times a_{\mathbf{p}+\mathbf{q},\gamma'_1}^+ a_{\mathbf{p}'-\mathbf{q},\gamma'_2}^+ a_{\mathbf{p}'\gamma_2} a_{\mathbf{p}\gamma_1}, \end{aligned} \quad (7)$$

where $a_{\mathbf{p}\gamma}$ is the destruction operator for electron with momentum \mathbf{p} from the band γ , $\xi_{p\gamma} = \gamma v_F p - \mu$ is its kinetic energy measured from the chemical potential μ and $V_{\mathbf{q}} = 2\pi e^2 / \varepsilon q$ is the two-dimensional Fourier transform of Coulomb interaction potential screened by surrounding three-dimensional medium with a dielectric susceptibility ε .

III. DESCRIPTION OF PLASMONS

To investigate the properties of plasmons in Dirac electron gas, we use equation-of-motion approach [25]. We treat a plasmon as a composite quasiparticle, consisting of electron-hole pairs with the common total momentum \mathbf{q} . Thus, the creation operator for plasmon with momentum \mathbf{q} can be written as:

$$Q_{\mathbf{q}}^+ = \sum_{\bar{\mathbf{p}}\gamma\gamma'} C_{\bar{\mathbf{p}}\mathbf{q}}^{\gamma'\gamma} a_{\bar{\mathbf{p}}+\mathbf{q},\gamma'}^+ a_{\mathbf{p}\gamma}. \quad (8)$$

Here the coefficients $C_{\bar{\mathbf{p}}\mathbf{q}}^{\gamma'\gamma}$ are the weights of intraband ($\gamma = \gamma'$) and interband ($\gamma \neq \gamma'$) single-particle transitions, contributing to the wave function of plasmon.

The plasmon creation operator should obey Heisenberg equation of motion

$$[H, Q_{\mathbf{q}}^+] = \Omega_{\mathbf{q}} Q_{\mathbf{q}}^+, \quad (9)$$

where $\Omega_{\mathbf{q}}$ is plasmon frequency. We start from equation of motion for single electron-hole pair, which can be derived using (7):

$$\begin{aligned} & [H, a_{\mathbf{p}+\mathbf{q},\gamma'}^+ a_{\mathbf{p}\gamma}] \\ &= (\xi_{\mathbf{p}+\mathbf{q},\gamma'} - \xi_{\mathbf{p}\gamma}) a_{\mathbf{p}+\mathbf{q},\gamma'}^+ a_{\mathbf{p}\gamma} + \frac{1}{S} \sum_{\mathbf{q}'} V_{\mathbf{q}'} \rho_{\mathbf{q}'}^+ \\ & \times \sum_{\gamma''} \left(\langle f_{\mathbf{p}+\mathbf{q}-\mathbf{q}',\gamma''} | f_{\mathbf{p}+\mathbf{q},\gamma'} \rangle a_{\mathbf{p}+\mathbf{q}-\mathbf{q}',\gamma''}^+ a_{\mathbf{p}\gamma} \right. \\ & \quad \left. - \langle f_{\mathbf{p}\gamma} | f_{\mathbf{p}+\mathbf{q}',\gamma''} \rangle a_{\mathbf{p}+\mathbf{q},\gamma'}^+ a_{\mathbf{p}+\mathbf{q}',\gamma''} \right), \end{aligned} \quad (10)$$

where we have introduced the Fourier transform of the density operator:

$$\rho_{\mathbf{q}}^+ = \sum_{\mathbf{p}\gamma\gamma'} \langle f_{\mathbf{p}+\mathbf{q},\gamma'} | f_{\mathbf{p}\gamma} \rangle a_{\mathbf{p}+\mathbf{q},\gamma'}^+ a_{\mathbf{p}\gamma}. \quad (11)$$

The right-hand side of the equation (10) contains products of four fermionic operators. To reduce it to products of two fermionic operators we use the random phase approximation (RPA); its applicability will be discussed below. According to RPA [25], the operator products in the last two lines of (10) can be replaced by their average values in ground state $|0\rangle$ of the system:

$$a_{\mathbf{p}\gamma'}^+ a_{\mathbf{p}\gamma} \rightarrow \langle 0 | a_{\mathbf{p}\gamma'}^+ a_{\mathbf{p}\gamma} | 0 \rangle = \delta_{\mathbf{p}\mathbf{p}'} \delta_{\gamma\gamma'} n_{\mathbf{p}\gamma}, \quad (12)$$

where $n_{\mathbf{p}\gamma}$ is the occupation number for electronic states with momentum \mathbf{p} from the band γ . For electron-doped

Dirac liquid at $T = 0$ (see also the remark at the end of this section), we have $n_{\mathbf{p}+} = \Theta(p_F - |\mathbf{p}|)$, $n_{\mathbf{p}-} = 1$, where $p_F = \mu/v_F$ is the Fermi momentum. In the case of hole doping, all characteristics of plasmons are the same due to electron-hole symmetry.

Thus, the equation of motion (10) for electron-hole pair with taking into account the RPA assumption (12) takes the form:

$$\left[H, a_{\mathbf{p}+\mathbf{q},\gamma'}^+ a_{\mathbf{p}\gamma} \right] = (\xi_{\mathbf{p}+\mathbf{q},\gamma'} - \xi_{\mathbf{p}\gamma}) a_{\mathbf{p}+\mathbf{q},\gamma'}^+ a_{\mathbf{p}\gamma} + \frac{V_q}{S} \rho_{\mathbf{q}}^+ \langle f_{\mathbf{p}\gamma} | f_{\mathbf{p}+\mathbf{q},\gamma'} \rangle (n_{\mathbf{p}\gamma} - n_{\mathbf{p}+\mathbf{q},\gamma'}). \quad (13)$$

Combining the definition of plasmon creation operator (8) with the equation of motion for plasmon (9) and single electron-hole pair (13), we obtain the system of equations for the coefficients $C_{\mathbf{p}\mathbf{q}}^{\gamma'\gamma}$:

$$(\Omega_q + \xi_{\mathbf{p}\gamma} - \xi_{\mathbf{p}+\mathbf{q},\gamma'}) C_{\mathbf{p}\mathbf{q}}^{\gamma'\gamma} = \frac{V_q}{S} \langle f_{\mathbf{p}+\mathbf{q},\gamma'} | f_{\mathbf{p}\gamma} \rangle + \sum_{\mathbf{p}'\tau\tau'} C_{\mathbf{p}'\mathbf{q}}^{\tau'\tau} \langle f_{\mathbf{p}'\tau} | f_{\mathbf{p}+\mathbf{q},\tau'} \rangle (n_{\mathbf{p}'\tau} - n_{\mathbf{p}'+\mathbf{q},\tau'}). \quad (14)$$

Introducing infinitesimal damping into the plasmon frequency and denoting

$$N_{\mathbf{q}} = \frac{V_q}{S} \sum_{\mathbf{p}\tau\tau'} C_{\mathbf{p}\mathbf{q}}^{\tau'\tau} \langle f_{\mathbf{p}\tau} | f_{\mathbf{p}+\mathbf{q},\tau'} \rangle (n_{\mathbf{p}\tau} - n_{\mathbf{p}+\mathbf{q},\tau'}), \quad (15)$$

we can find the plasmon wave function from (14) as:

$$C_{\mathbf{p}\mathbf{q}}^{\gamma'\gamma} = \frac{\langle f_{\mathbf{p}+\mathbf{q},\gamma'} | f_{\mathbf{p}\gamma} \rangle N_{\mathbf{q}}}{\Omega_q + \xi_{\mathbf{p}\gamma} - \xi_{\mathbf{p}+\mathbf{q},\gamma'} + i\delta}. \quad (16)$$

The normalization factor $N_{\mathbf{q}}$ can be determined from the commutation relation for plasmon operators, which should be satisfied on the average in the ground state:

$$\langle 0 | [Q_{\mathbf{q}}, Q_{\mathbf{q}'}^+] | 0 \rangle = \delta_{\mathbf{q}\mathbf{q}'}. \quad (17)$$

Substituting (8) in (17), we get

$$\sum_{\gamma\gamma'} D_{\gamma'\gamma} = 1, \quad (18)$$

where the total weights of intraband (D_{++}) and interband ($D_{+-} + D_{-+} = 1 - D_{++}$) electron transitions, contributing to the plasmon wave function (16), are:

$$D_{\gamma'\gamma} = \sum_{\mathbf{p}} \left| C_{\mathbf{p}\mathbf{q}}^{\gamma'\gamma} \right|^2 (n_{\mathbf{p}\gamma} - n_{\mathbf{p}+\mathbf{q},\gamma'}). \quad (19)$$

To find the plasmon frequency Ω_q , we can substitute (16) in (15), arriving to the standard RPA equation (see it for the helical liquid [11] and for graphene [18, 19]):

$$1 - V_q \Pi(q, \Omega_q) = 0, \quad (20)$$

where the polarization operator of Dirac electron gas is introduced:

$$\Pi(q, \omega) = \frac{g}{S} \sum_{\mathbf{p}\gamma\gamma'} |\langle f_{\mathbf{p}+\mathbf{q},\gamma'} | f_{\mathbf{p}\gamma} \rangle|^2 \times \frac{n_{\mathbf{p}\gamma} - n_{\mathbf{p}+\mathbf{q},\gamma'}}{\omega + \xi_{\mathbf{p}\gamma} - \xi_{\mathbf{p}+\mathbf{q},\gamma'} + i\delta}. \quad (21)$$

The degeneracy factor g is 1 for helical liquid on the surface of topological insulator and 4 for graphene. The angular factors $\langle f_{\mathbf{p}+\mathbf{q},\gamma'} | f_{\mathbf{p}\gamma} \rangle$ are specific to chiral Dirac electron and arise in (21) as a result of summation over spinor components of electron wave function.

The random phase approximation becomes exact in the limit of small values of dimensional parameter r_s , defined as a ratio of characteristic Coulomb interaction energy to kinetic energy. For the gas of massless particles, r_s does not depend on electron density and equals to $r_s = e^2/\varepsilon v_F$ (effectively, $\varepsilon = (\varepsilon_1 + \varepsilon_2)/2$ when two-dimensional electron layer is surrounded by two dielectric half-spaces with susceptibilities ε_1 and ε_2). For Bi_2Se_3 , $r_s = 0.09$ with $\varepsilon = 40$ for dielectric half-space, and applicability of the RPA is well established (the value of r_s for another material Bi_2Te_3 is close to that for Bi_2Se_3). In the case of graphene, r_s is not small, but applicability of the RPA can be established due to smallness of the parameter $1/g$, leading to selection of bubble diagrams (see [16] and references therein, and also the work [26]).

Maximal achievable amounts of doping of helical liquid on a surface of Bi_2Se_3 are $\mu \sim 0.3$ eV [24], therefore at room temperature it can be degenerate electron liquid. Hence we assume that $T = 0$ in all calculations below.

IV. WAVE FUNCTION OF PLASMON

Plasmon dispersions Ω_q , calculated numerically from (20)–(21) at various r_s , are plotted in Fig. 1. We also present results for suspended graphene with $r_s = 8.8$ ($\varepsilon = 1$) and for graphene embedded into SiO_2 environment with $r_s = 2.2$ ($\varepsilon = 4$). For convenience, the degeneracy factor $g = 4$ is included here into r_s , since the plasmon dispersion in RPA (20) depend only on the combination gr_s .

It is seen that for small values of r_s (the case of topological insulator) the plasmon dispersion law approaches very closely to the upper border of the continuum of intraband single-particle transitions ($\omega < v_F q$). On the contrary, at moderate and large r_s , plasmon has well-defined square-root dispersion in the long-wavelength range. At $q \approx p_F$, the plasmon enters the continuum of interband single-particle transitions ($\omega > 2\mu - v_F q$). Inside the single-particle continuum, energy and momentum conservation laws allow energy transfer between plasmon and single-particle excitations, so the plasmon acquires a finite lifetime.

The internal structure of plasmons in Dirac electron gas can be investigated by looking at total weights (19) of intra- and interband transitions in its wave function.

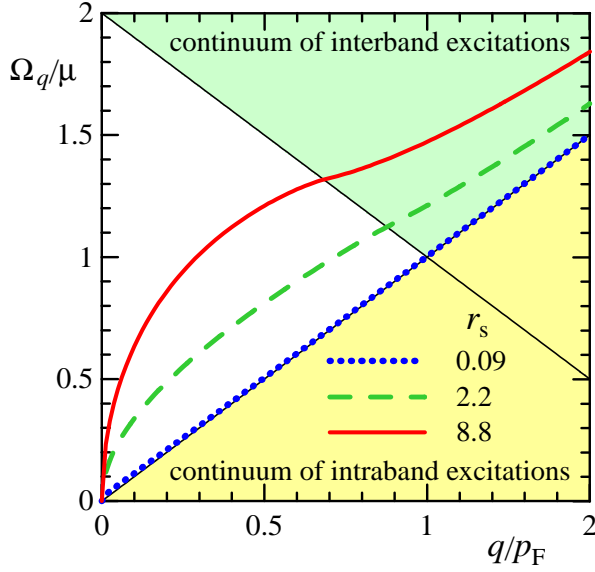


FIG. 1. Plasmon dispersions Ω_q at different values of r_s . Continuums of intraband ($\omega < v_F q$) and interband ($\omega > 2\mu - v_F q$) single-particle excitations are shaded; $p_F = \mu/v_F$ is the Fermi momentum, μ is the chemical potential.

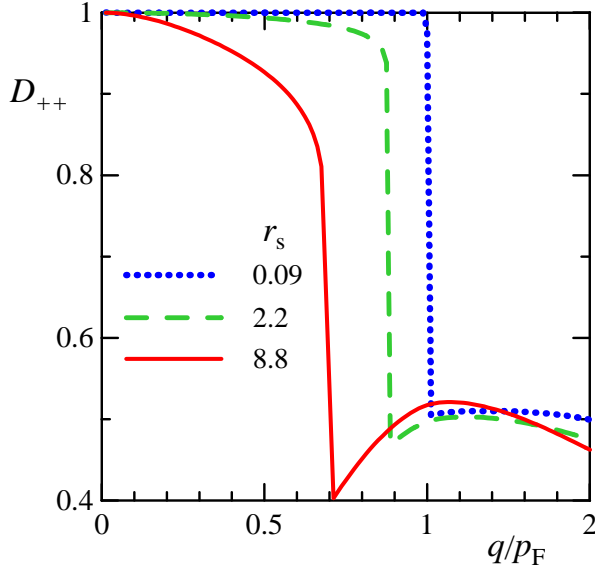


FIG. 2. Weight D_{++} (19) of intraband electron-hole transitions in plasmon wave function at different values of r_s .

The weight D_{++} of intraband single-particle transitions is plotted in Fig. 2. It is seen that the undamped plasmon for all values of parameter r_s consists mainly of intraband transitions, thus an influence of valence band on its properties is rather weak. When the plasmon enters the single-particle continuum, inter- and intraband transitions start to contribute almost equally to its wave function, but the plasmon undergoes strong Landau damping.

The detailed picture of the plasmon wave function in momentum space $C_{\mathbf{p}\mathbf{q}}^{\gamma'\gamma}$, showing the distribution of con-

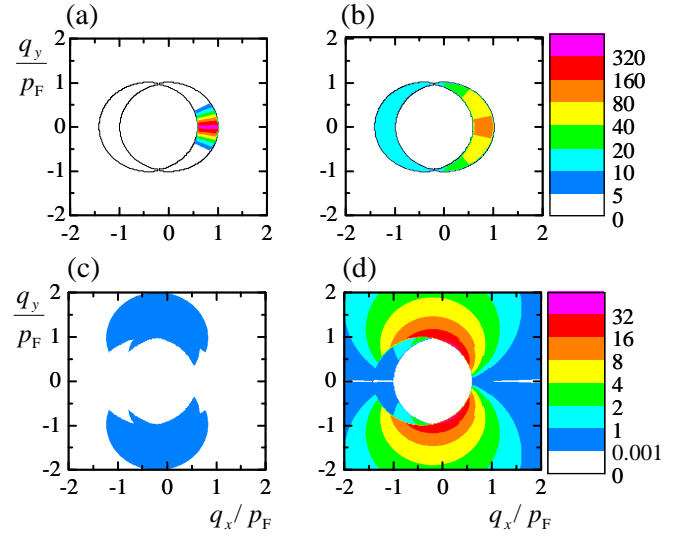


FIG. 3. Squared modulus of plasmon wave function $|C_{\mathbf{p}\mathbf{q}}^{\gamma'\gamma}|^2$ on the plane of the hole momentum \mathbf{p} at $q = 0.4p_F$. Top row: intraband channel $|C_{\mathbf{p}\mathbf{q}}^{++}|^2$ at $r_s = 0.09$ (a) and $r_s = 8.8$ (b). Bottom row: interband channel $|C_{\mathbf{p}\mathbf{q}}^{+-}|^2 + |C_{\mathbf{p}\mathbf{q}}^{-+}|^2$ at $r_s = 0.09$ (c) and $r_s = 8.8$ (d).

tributions of intraband $|C_{\mathbf{p}\mathbf{q}}^{++}|^2$ or interband $|C_{\mathbf{p}\mathbf{q}}^{+-}|^2 + |C_{\mathbf{p}\mathbf{q}}^{-+}|^2$ electron-hole pairs into wave function of plasmon with given momentum q is presented in Fig. 3. The results are calculated for $q = 0.4p_F$ at $r_s = 0.09$ and 8.8 . For other values of plasmon momentum q , the results are qualitatively similar. It is seen that for small values of r_s (the case of topological insulator) the distribution of intraband contributions is very sharply peaked in the forward direction, whereas the contribution of interband transitions is negligible. It can be understood from the reason that the plasmon dispersion is very close to the single-particle continuum (see Fig. 1) and thus the plasmon itself behave almost as single intraband electron-hole transition.

At large values of parameter r_s (the case of suspended graphene), the broad range of electron intraband transitions in momentum space contribute to plasmon. The weight of interband transitions is small but not negligible. Contributions of interband transitions form two side lobes, since the angular factor $\langle f_{\mathbf{p}+\mathbf{q},\pm} | f_{\mathbf{p}\mp} \rangle$ suppresses interband forward scattering.

V. CHARGE- AND SPIN-DENSITY WAVES

When a spin-plasmon is excited in the helical liquid, anisotropic distribution of electron-hole pairs of the type, depicted in Fig. 3, arises. This distribution is shifted towards the plasmon momentum \mathbf{q} . Due to the spin-momentum locking, the system should acquire a total nonzero spin polarization, perpendicular to \mathbf{q} . A similar situation occurs in the current-carrying state of the helical liquid, which turns out to be spin-polarized [9].

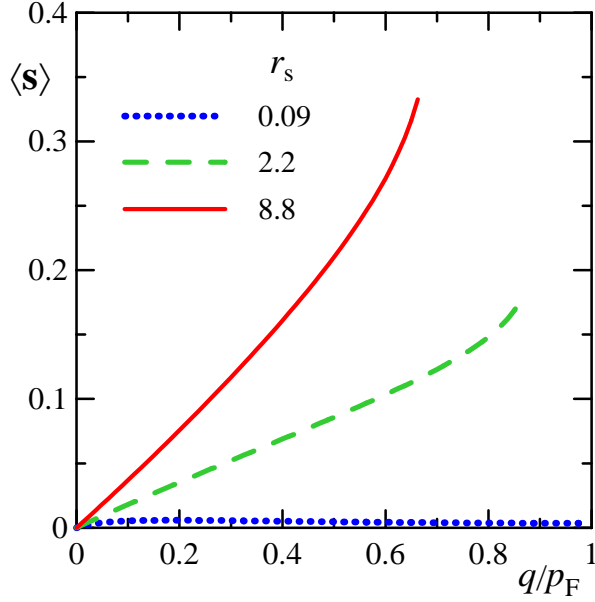


FIG. 4. In-plane transverse spin polarization of the system $\langle \mathbf{s} \rangle$ (22) in the state with single spin-plasmon excited as function of its momentum q at different values of r_s .

Average of spin polarization in the state $|1_{\mathbf{q}}\rangle = Q_{\mathbf{q}}^+|0\rangle$ with a single plasmon excited is $\langle \mathbf{s} \rangle = \langle 1_{\mathbf{q}} | \boldsymbol{\sigma} / 2 | 1_{\mathbf{q}} \rangle$ and can be calculated using (8) as:

$$\langle \mathbf{s} \rangle = \frac{1}{2} \sum_{\mathbf{p}\gamma\gamma'\tau} \left[\langle f_{\mathbf{p}+\mathbf{q},\gamma'} | \boldsymbol{\sigma} | f_{\mathbf{p}+\mathbf{q},\tau} \rangle C_{\mathbf{p}\mathbf{q}}^{\tau\gamma} - C_{\mathbf{p}\mathbf{q}}^{\gamma'\tau} \langle f_{\mathbf{p}\tau} | \boldsymbol{\sigma} | f_{\mathbf{p}\gamma} \rangle \right] \left(C_{\mathbf{p}\mathbf{q}}^{\gamma'\gamma} \right)^* (n_{\mathbf{p}\gamma} - n_{\mathbf{p}+\mathbf{q},\gamma'}). \quad (22)$$

If \mathbf{q} is parallel to \mathbf{e}_x , only the y -component of $\langle \mathbf{s} \rangle$ is nonzero. Its dependence on q for undamped plasmons at various r_s is plotted in Fig. 4. At large enough r_s , the spin polarization of the system is comparable to the whole spin of a single electron.

Note that in the case of graphene the isospin polarization of the system appears instead of spin polarization. Isospin polarization corresponds to nonzero average phase shift between wave function of electrons on different sublattices. On the contrary, in pseudospin-unpolarized state this shift is zero on the average.

In ordinary electronic system without spin-momentum coupling caused by spin-orbit interaction, plasmon manifests itself as charge-density wave. In helical liquid on surface of topological insulator, due to the spin-momentum locking, spin-plasmon manifests itself as coupled charge- and spin-density waves. These waves, accompanying spin-plasmon with the momentum \mathbf{q} , can be characterized by corresponding spatial harmonics of charge- (11) and spin-density

$$\mathbf{s}_{\mathbf{q}}^+ = \frac{1}{2} \sum_{\mathbf{p}\gamma\gamma'} \langle f_{\mathbf{p}+\mathbf{q},\gamma'} | \boldsymbol{\sigma} | f_{\mathbf{p}\gamma} \rangle a_{\mathbf{p}+\mathbf{q},\gamma'}^+ a_{\mathbf{p}\gamma} \quad (23)$$

operators.

To relate these quantities to the plasmon operators (8), we employ the unitary transformation, connecting operators of electron-hole excitations in noninteracting system $a_{\mathbf{p}+\mathbf{q},\gamma'}^+, a_{\mathbf{p}\gamma}$ with operators of plasmons $Q_{\mathbf{q}}^+$. For this purpose, we also need explicit expressions for operators of distorted single-particle excitations in the system with Coulomb interaction (similarly to the work [27]). Denoting creation operator for such single-particle excitation with total momentum \mathbf{q} and energy $\xi_{\mathbf{p}+\mathbf{q},\gamma'} - \xi_{\mathbf{p}\gamma}$ as $\eta_{\mathbf{p}\mathbf{q}\gamma\gamma'}^+$, we can use the equation-of-motion method in the RPA and, similarly to the case of plasmons, get the explicit expression for it:

$$\eta_{\mathbf{p}\mathbf{q}\gamma\gamma'}^+ = \sum_{\mathbf{p}'\tau\tau'} U_{\mathbf{p}\mathbf{p}'\mathbf{q}}^{\gamma\gamma'\tau\tau'} a_{\mathbf{p}'+\mathbf{q},\tau'}^+ a_{\mathbf{p}'\tau}, \quad (24)$$

where

$$U_{\mathbf{p}\mathbf{p}'\mathbf{q}}^{\gamma\gamma'\tau\tau'} = \delta_{\mathbf{p}\mathbf{p}'} \delta_{\gamma\gamma'} \delta_{\tau\tau'} + \frac{V_q}{S} \frac{\langle f_{\mathbf{p}\gamma} | f_{\mathbf{p}+\mathbf{q},\gamma'} \rangle (n_{\mathbf{p}\gamma} - n_{\mathbf{p}+\mathbf{q},\gamma'})}{1 - V_q \Pi(q, \xi_{\mathbf{p}+\mathbf{q},\gamma'} - \xi_{\mathbf{p}\gamma})} \times \frac{\langle f_{\mathbf{p}'+\mathbf{q},\tau'} | f_{\mathbf{p}'\tau} \rangle}{\xi_{\mathbf{p}'\tau} - \xi_{\mathbf{p}'+\mathbf{q},\tau'} - \xi_{\mathbf{p}\gamma} + \xi_{\mathbf{p}+\mathbf{q},\gamma'} + i\delta}. \quad (25)$$

The expressions (8), (16), (24) and (25) establish the unitary transformation at given \mathbf{q} from operators of electron-hole excitations in noninteracting system $a_{\mathbf{p}+\mathbf{q},\gamma'}^+, a_{\mathbf{p}\gamma}$ to operators of excitations in Coulomb-interacting system: plasmons $Q_{\mathbf{q}}^+$ and single-particle excitations $\eta_{\mathbf{p}\mathbf{q}\gamma\gamma'}^+$. We can easily derive the inverse transformation of the form:

$$a_{\mathbf{p}+\mathbf{q},\gamma'}^+ a_{\mathbf{p}\gamma} = (n_{\mathbf{p}\gamma} - n_{\mathbf{p}+\mathbf{q},\gamma'}) \times \left\{ (C_{\mathbf{p}\mathbf{q}}^{\gamma'\gamma})^* Q_{\mathbf{q}}^+ + \sum_{\mathbf{p}'\tau\tau'} (U_{\mathbf{p}\mathbf{p}'\mathbf{q}}^{\tau\tau'\gamma\gamma'})^* \eta_{\mathbf{p}'\mathbf{q}\tau\tau'}^+ \right\}. \quad (26)$$

According to (26), we can represent the operators (11) and (23) of charge- and spin-density waves in the form:

$$\rho_{\mathbf{q}}^+ = S N_{\mathbf{q}}^* \Pi(q, \Omega_q) Q_{\mathbf{q}}^+ + \tilde{\rho}_{\mathbf{q}}^+, \quad (27)$$

$$\mathbf{s}_{\mathbf{q}}^+ = S N_{\mathbf{q}}^* \boldsymbol{\Pi}_s(q, \Omega_q) Q_{\mathbf{q}}^+ + \tilde{\mathbf{s}}_{\mathbf{q}}^+, \quad (28)$$

where the parts $\tilde{\rho}_{\mathbf{q}}^+$ and $\tilde{\mathbf{s}}_{\mathbf{q}}^+$ are the contributions of single-particle excitations and are dynamically independent on plasmons. Here, along with the usual susceptibility (21), the crossed spin-density susceptibility of the helical liquid [11] has been introduced:

$$\boldsymbol{\Pi}_s(q, \omega) = \frac{1}{2S} \sum_{\mathbf{p}\gamma\gamma'} \langle f_{\mathbf{p}+\mathbf{q},\gamma'} | f_{\mathbf{p}\gamma} \rangle \times \langle f_{\mathbf{p}\gamma} | \boldsymbol{\sigma} | f_{\mathbf{p}+\mathbf{q},\gamma'} \rangle \frac{n_{\mathbf{p}\gamma} - n_{\mathbf{p}+\mathbf{q},\gamma'}}{\omega + \xi_{\mathbf{p}\gamma} - \xi_{\mathbf{p}+\mathbf{q},\gamma'} + i\delta}. \quad (29)$$

The formulas (27)–(28) show us that the average values of $\rho_{\mathbf{q}}^+$ and $\mathbf{s}_{\mathbf{q}}^+$ in any state with a definite number of plasmons vanish (similarly to the mean value of coordinate or momentum in the simplest quantum harmonic

oscillator). However, we can calculate their mean squares in the $n_{\mathbf{q}}$ -plasmon state $|n_{\mathbf{q}}\rangle = [(Q_{\mathbf{q}}^+)^{n_{\mathbf{q}}} / (n_{\mathbf{q}}!)^{-1/2}]|0\rangle$:

$$\langle \rho_{\mathbf{q}} \rho_{\mathbf{q}}^+ \rangle \equiv \langle n_{\mathbf{q}} | \rho_{\mathbf{q}} \rho_{\mathbf{q}}^+ | n_{\mathbf{q}} \rangle - \langle 0 | \rho_{\mathbf{q}} \rho_{\mathbf{q}}^+ | 0 \rangle, \quad (30)$$

$$\langle s_{\mathbf{q}}^{\perp} (s_{\mathbf{q}}^{\perp})^+ \rangle \equiv \langle n_{\mathbf{q}} | s_{\mathbf{q}}^{\perp} (s_{\mathbf{q}}^{\perp})^+ | n_{\mathbf{q}} \rangle - \langle 0 | s_{\mathbf{q}}^{\perp} (s_{\mathbf{q}}^{\perp})^+ | 0 \rangle \quad (31)$$

(only the in-plane transverse component s^{\perp} of the spin \mathbf{s} is nonzero upon averaging). Since we are interested in plasmons only, we have subtracted the vacuum fluctuations of these quantities in the ground state $|0\rangle$.

Using (27)–(28), the mean squares of charge- and spin-density wave amplitudes (30)–(31) can easily be calculated:

$$\langle \rho_{\mathbf{q}} \rho_{\mathbf{q}}^+ \rangle = n_{\mathbf{q}} S^2 |N_{\mathbf{q}} \Pi(q, \Omega_q)|^2, \quad (32)$$

$$\langle s_{\mathbf{q}}^{\perp} (s_{\mathbf{q}}^{\perp})^+ \rangle = n_{\mathbf{q}} S^2 |N_{\mathbf{q}} \Pi_s^{\perp}(q, \Omega_q)|^2. \quad (33)$$

We can normalize the amplitudes to obtain dimensionless quantities $A_{\rho}(q) = [\langle \rho_{\mathbf{q}} \rho_{\mathbf{q}}^+ \rangle / n_{\mathbf{q}} S \rho]^{1/2}$ and $A_s(q) = [\langle s_{\mathbf{q}}^{\perp} (s_{\mathbf{q}}^{\perp})^+ \rangle / n_{\mathbf{q}} S \rho]^{1/2}$ ($\rho = p_F^2 / 4\pi$ is the average electron density), plotted in Fig. 5. As seen, the amplitudes of charge- and spin-density waves are close quantitatively at moderate momenta and any r_s .

In [11], it was shown that, due to spin-momentum locking, electron density and transverse component of spin obey an analogue of “continuity equation”. It requires that

$$\Omega_q A_{\rho}(q) = 2v_F q A_s(q). \quad (34)$$

Our results are in agreement with this equation.

VI. SPIN-PLASMON SCATTERING

Nontrivial internal structure of plasmon in Dirac electron gas can reveal itself in a process of its scattering on external potentials or impurities. For the case of spin-plasmon, it is also interesting to consider its scattering on magnetic field, acting on electron spins. Since we are interested in spin effects here, we will consider only in-plane magnetic field, affecting only spins of electrons and not their orbital motion.

Hamiltonian of interaction of electrons in helical liquid with external electric $U(\mathbf{r})$ and magnetic $\mathbf{H}(\mathbf{r})$ fields are, respectively,

$$H_e = -e \sum_{\mathbf{p}\mathbf{p}'\gamma\gamma'} U_{\mathbf{p}'-\mathbf{p}} \langle f_{\mathbf{p}'\gamma'} | f_{\mathbf{p}\gamma} \rangle a_{\mathbf{p}'\gamma'}^+ a_{\mathbf{p}\gamma}, \quad (35)$$

$$H_m = \mu_B \sum_{\mathbf{p}\mathbf{p}'\gamma\gamma'} \mathbf{H}_{\mathbf{p}'-\mathbf{p}} \langle f_{\mathbf{p}'\gamma'} | \boldsymbol{\sigma} | f_{\mathbf{p}\gamma} \rangle a_{\mathbf{p}'\gamma'}^+ a_{\mathbf{p}\gamma}, \quad (36)$$

where $U_{\mathbf{q}}$ and $\mathbf{H}_{\mathbf{q}}$ are Fourier components of external electric and magnetic fields, $\mu_B = e/2mc$ is the Bohr magneton.

To calculate the probability of elastic scattering of the spin-plasmon with initial momentum \mathbf{q} to the state with the final momentum \mathbf{q}' , we can use the Fermi golden rule,

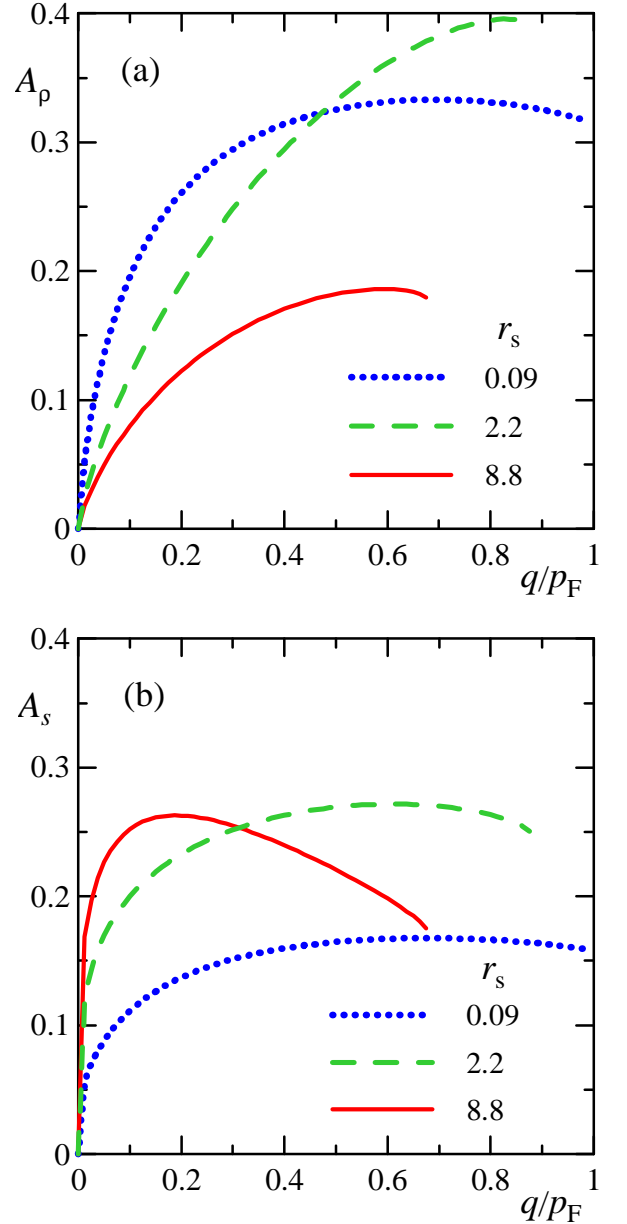


FIG. 5. Normalized amplitudes of charge-density A_{ρ} (a) and spin-density A_s (b) waves in many-plasmon state as function of plasmons momentum q at different values of r_s .

corresponding to the Born approximation. Thus, the differential (with respect to the scattering angle) probabilities of this scattering on electric and magnetic fields can be presented in the following form:

$$\frac{dw_e}{d\theta} = |V_{\mathbf{q}'-\mathbf{q}}|^2 |\Phi_e(q, \theta)|^2, \quad (37)$$

$$\frac{dw_m}{d\theta} = |\mathbf{H}_{\mathbf{q}'-\mathbf{q}} \cdot \boldsymbol{\Phi}_m(q, \theta)|^2, \quad (38)$$

where θ is scattering angle (i.e. the angle between \mathbf{q} and \mathbf{q}'); q is absolute value of both \mathbf{q} and \mathbf{q}' . Here we have introduced electric $\Phi_e(q, \theta)$ and magnetic $\boldsymbol{\Phi}_m(q, \theta)$ form-factors of spin-plasmon.

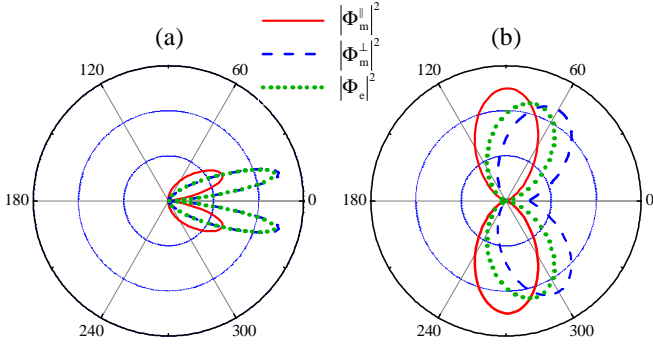


FIG. 6. Polar graphs of the squared modulus of electric $|\Phi_e(q, \theta)|^2$ and components $|\Phi_m^{\parallel}(q, \theta)|^2$, $|\Phi_m^{\perp}(q, \theta)|^2$ of magnetic form-factor of spin-plasmon with the momentum $q = 0.6p_F$ at $r_s = 0.09$ (a) and $r_s = 8.8$ (b).

Using (35)–(36), we can calculate the form-factors explicitly:

$$\begin{aligned} \Phi_e(q, \theta) = & e \sqrt{\frac{q}{\Omega'_q}} \sum_{\mathbf{p}\gamma\gamma'\tau} (\langle f_{\mathbf{p}+\mathbf{q}',\gamma'} | f_{\mathbf{p}+\mathbf{q},\tau} \rangle \\ & \times C_{\mathbf{p}\mathbf{q}}^{\tau\gamma} - C_{\mathbf{p}+\mathbf{q}'-\mathbf{q},\mathbf{q}}^{\gamma'\tau} \langle f_{\mathbf{p}+\mathbf{q}'-\mathbf{q},\tau} | f_{\mathbf{p}\gamma} \rangle) \\ & \times (C_{\mathbf{p}\mathbf{q}}^{\gamma'\tau})^* (n_{\mathbf{p}\gamma} - n_{\mathbf{p}+\mathbf{q}'\gamma'}), \quad (39) \end{aligned}$$

$$\begin{aligned} \Phi_m(q, \theta) = & \mu_B \sqrt{\frac{q}{\Omega'_q}} \sum_{\mathbf{p}\gamma\gamma'\tau} (\langle f_{\mathbf{p}+\mathbf{q}',\gamma'} | \sigma | f_{\mathbf{p}+\mathbf{q},\tau} \rangle \\ & \times C_{\mathbf{p}\mathbf{q}}^{\tau\gamma} - C_{\mathbf{p}+\mathbf{q}'-\mathbf{q},\mathbf{q}}^{\gamma'\tau} \langle f_{\mathbf{p}+\mathbf{q}'-\mathbf{q},\tau} | \sigma | f_{\mathbf{p}\gamma} \rangle) \\ & \times (C_{\mathbf{p}\mathbf{q}}^{\gamma'\tau})^* (n_{\mathbf{p}\gamma} - n_{\mathbf{p}+\mathbf{q}'\gamma'}). \quad (40) \end{aligned}$$

Here $\Omega'_q = d\Omega_q/dq$ is the derivative of spin-plasmon dispersion law. It is convenient to project the vector Φ_m on directions, parallel and perpendicular to the initial plasmon momentum \mathbf{q} to get Φ_m^{\parallel} and Φ_m^{\perp} respectively.

We consider only the form-factors, revealing the specifics of spin-plasmons, instead of the whole differential probabilities (37)–(38), also dependent on the form of external field. In Fig. 6, angle dependencies of squared modulus $|\Phi_e(q, \theta)|^2$, $|\Phi_m^{\parallel}(q, \theta)|^2$ and $|\Phi_m^{\perp}(q, \theta)|^2$ of the form-factors at $q = 0.6p_F$ are plotted; these angular distributions are normalized to unity. In their calculation, we have used the single-band approximation, since undamped plasmons consist mainly of interband transitions, according to Fig. 2. Results for other values of plasmon momentum are qualitatively the same.

In the case of forward scattering with zero momentum transfer (at $\theta = 0$), the external electric field probes the total charge of plasmon, which is actually zero. Thus, the corresponding electric form-factor $\Phi_e(q, 0) = 0$. Similarly, forward scattering on magnetic field probes the total spin of spin-plasmon, which is directed perpendicularly to \mathbf{q} . Therefore, $\Phi_m^{\parallel}(q, 0) = 0$ and $\Phi_m^{\perp}(q, 0) \neq 0$. As for backscattering of plasmon, it is strictly prohibited, as for individual massless Dirac electrons [28].

As seen in Fig. 6, the form-factors demonstrate two side lobes, rather sharp at small r_s , which can be considered as a consequence of sharp peaking of the plasmon wave function (see Fig. 3). At large r_s , these lobes are much broader.

In the process of spin-plasmon scattering on some configurations of electric or magnetic fields, we can expect interplay between spatial structure of these fields and that of the spin-plasmon. Angular distribution of the scattered plasmons will incorporate both of these factors, according to (37)–(38). Controlling the overlap of maxima of external potential and spin-plasmon form-factors, one can manipulate spin-plasmon scattering.

Magnetic or nonmagnetic impurities can also create the external field. If the characteristic radius of the impurity potential is R , the transferred momentum will be limited by R^{-1} by the order of magnitude. If $qR \gg 1$, the plasmon scattering on impurities will be suppressed due to proximity to the regime of forward scattering. In the opposite limit $qR \ll 1$, plasmons will be effectively scattered on considerable angles.

VII. CONCLUSIONS

The properties of collective excitations (plasmons or spin-plasmons) in two-dimensional gas of massless Dirac particles were studied. Two physical realizations of such systems were considered: electron gas in graphene and helical liquid on the surface of topological insulator. Quantum field-theoretical formalism for comprehensive description of spin-plasmons as composite Bose particles in the random phase approximation was developed. Internal structure and wave function of spin-plasmons were studied.

Signatures of spin-momentum locking in helical liquid were considered. In particular, it was shown that excitation of a spin-plasmon induces the total nonzero spin polarization of the system. Moreover, coupling between charge- and spin-density waves, accompanying a spin-plasmon, was demonstrated. It was shown that amplitudes of both of these waves are close by the order of magnitude for spin-plasmons of intermediate momenta. The results of this work can be confirmed by experiments involving spin-plasmon excitation on the surface of topological insulator and independent measurements of charge and spin wave amplitudes (one of experiments of this type was proposed in [11]). The similar effect of coupling between charge and spin appears in electron gas with spin-orbit coupling [29], but amplitude of spin wave is considerable less in this case than that of charge waves for experimentally relevant parameters.

Elastic scattering of spin-plasmons in helical liquid on electric and magnetic external fields is considered. Angular distribution of scattered spin-plasmons depend on both the shape of the potential and the form-factor of the spin-plasmon, revealing its internal structure. It was shown that, due to the form-factor, the scattering occurs

into two side lobes, while forward and backward scattering is suppressed. One can use this fact to manipulate spin-plasmon scattering via interplay between plasmon form-factor and form-factor of the external potential. It can be also concluded that scattering of spin-plasmons on long-range impurities should be very weak.

Coupling between charge and spin waves, demonstrated in this article, can be used for realization of various spintronic devices. One can perform controllable focusing of spin-plasmon waves and thus create regions with high spin polarization. Spin-polarized electrons, accumulating in these regions, can diffuse to adjacent electrodes and be used to drive spin currents (similarly to [12]).

The quantum field-theoretical approach, presented in this article, can be used for theoretical description of an influence of various external factors (impurities, external fields) on plasmons in Dirac electron gas. The problems of two-dimensional spin-plasmon optics, based on ma-

nipulations by inhomogeneities of the system and three-dimensional environment, can be solved. Also the properties of hybrid modes (plasmon polaritons [30], plasmon-phonon modes [21, 22], plasmon-hole modes — plasmarons [31]) can be studied using this approach.

The classical electrodynamic approach based on Maxwell equations and response functions cannot describe quantum effects, arising when individual plasmons are emitted and adsorbed. Therefore, the quantum field-theoretical approach, presented in this article, should be especially useful for the problems of quantum plasmonics, which seems to be rather feasible in graphene-based structures [23].

The work was supported by Russian Foundation for Basic Research (grants 11-02-12209-ofi-m and 10-02-92607-KO_a) and by Grant of the President of Russian Federation MK-5288.2011.2. One of the authors (AAS) acknowledges support from the Dynasty Foundation.

-
- [1] M Z Hasan and C L Kane, “Topological insulators,” *Rev. Mod. Phys.* **82**, 3045–3067 (2010).
 - [2] X L Qi and S C Zhang, “The quantum spin hall effect and topological insulators,” *Physics Today* **63**, 33–37 (2010).
 - [3] X L Qi, T L Hughes, and S C Zhang, “Topological field theory of time-reversal invariant insulators,” *Phys. Rev. B* **78**, 195424–195467 (2009).
 - [4] A M Essin, J E Moore, and D Vanderbilt, “Magnetoelectric polarizability and axion electrodynamics in crystalline insulators,” *Phys. Rev. Lett.* **102**, 146805–146809 (2009).
 - [5] Y L Chen, J G Analytis, Z H Chu, Z K Liu, S K Mo, X L Qi, H J Zhang, D H Lu, X Dai, Z Fang, S C Zhang, I R Fisher, Z Hussain, and Z X Shen, “Large gap topological insulator Bi_2Te_3 with a single dirac cone on the surface,” *Science* **325**, 178–182 (2009).
 - [6] D Hsieh, Y Xia, D Qian, L Wray, F Dil, Z Hand Meier, J Osterwalder, J G Patthey, L Checkelsky, NP Ong, H Fedorov, AV Lin, A Bansil, D Grauer, Y S Hor, R J Cava, and M Z Hasan, “First observation of spin-momentum helical locking in Bi_2Se_3 and Bi_2Te_3 , demonstration of topological-order at 300k and a realization of topological-transport-regime,” *Nature* **460**, 1101–1105 (2009).
 - [7] Y Xia, L Wray, D Qian, D Hsieh, A Pal, H Lin, A Bansil, D Grauer, Y Hor, R Cava, and M Z Hasan, “Discovery (theoretical prediction and experimental observation) of a large-gap topological-insulator class with spin-polarized single-dirac-cone on the surface,” *Nature Phys.* **5**, 398–402 (2009).
 - [8] A A Burkov and D G Hawthorn, “Spin and charge transport on the surface of a topological insulator,” *Phys. Rev. Lett.* **105**, 066802–066806 (2010).
 - [9] D Culcer, E H Hwang, D T Stanescu, and S Das Sarma, “Two-dimensional surface charge transport in topological insulators,” *Rev. Mod. Phys.* **82**, 155457–155474 (2010).
 - [10] T Yokoyama, Y Tanaka, , and N Nagaosa, “Giant spin rotation in the junction between a normal metal and a quantum spin hall system,” *Phys. Rev. Lett.* **102**, 166801–166805 (2009).
 - [11] S Raghu, S B Chung, X L Qi, and S C Zhang, “Collective modes of a helical liquid,” *Phys. Rev. Lett.* **104**, 116401–116405 (2010).
 - [12] I Appelbaum, H D Drew, and M S Fuhrer, “Proposal for a topological plasmon spin rectifier,” *Appl. Phys. Lett.* **98**, 023103–023107 (2011).
 - [13] A Karch, “Surface plasmons and topological insulators,” (2011), [arXiv:1104.4125v2](https://arxiv.org/abs/1104.4125v2).
 - [14] K S Novoselov, A K Geim, S V Morozov, D Jiang, Y Zhang, S V Dubonos, I V Grigorieva, and A A Firsov, “Electric field effects in atomically thin carbon films,” *Science* **306**, 666–670 (2004).
 - [15] K S Novoselov, A K Geim, S V Morozov, D Jiang, M I Katsnelson, I V Grigorieva, S V Dubonos, and A A Firsov, “Two-dimensional gas of massless dirac fermions in graphene,” *Nature* **438**, 197–201 (2005).
 - [16] A H Castro Neto, F Guinea, N M R Peres, K S Novoselov, and A K Geim, “Electronic properties of graphene,” *Rev. Mod. Phys.* **81**, 109–162 (2009).
 - [17] V N Kotov, B Uchoa, V M Pereira, A H Castro Neto, and F Guinea, “Electron-electron interactions in graphene: Current status and perspectives,” (2011), [arXiv:1012.3484v1](https://arxiv.org/abs/1012.3484v1).
 - [18] E H Hwang and S Das Sarma, “Dielectric function, screening, and plasmons in 2d graphene,” *Phys. Rev. B* **75**, 205418–672 (2007).
 - [19] B Wunsch, T Stauber, F Sols, and F Guinea, “Dynamical polarization of graphene at finite doping,” *New J Phys* **8**, 318–333 (2006).
 - [20] Y u V Bludov, M I Vasilevskiy, and N M R Peres, “Mechanism for graphene-based optoelectronic switches by tuning surface plasmon-polaritons in monolayer,” *Europhysics Letters* **92**, 68001–68006 (2010).
 - [21] E H Hwang, R Sensarma, and S Das Sarma, “Plasmon-phonon coupling in graphene,” *Phys. Rev. B* **82**, 195406–195411 (2010).
 - [22] Y u Liu and R F Willis, “Plasmon-phonon strongly-coupled mode in epitaxial graphene,” *Phys Rev B.* **81**, 081406–081410 (2010).

- [23] F H L Koppens, D E Chang, and F J G de Abajo, “Graphene plasmonics: A platform for strong light-matter interaction,” (2011), [arXiv:1104.2068](#).
- [24] H Zhang, C X Liu, X L Qi, X Dai, Z Fang, and S C Zhang, “Topological insulators in Bi_2Se_3 , Bi_2Te_3 and Sb_2Te_3 with a single dirac cone on the surface,” *Nature Phys.* **5**, 438–442 (2009).
- [25] K Sawada, K A Brueckner, N Fukuda, and R Brout, “Correlation energy of an electron gas at high density: plasma oscillations,” *Phys. Rev.* **108**, 507–514 (1957).
- [26] S M Apenko, D A Kirzhnits, and Yu E Lozovik, “On the validity of the $1/n$ -expansion,” *Phys. Lett. A* **92**, 107–109 (1982).
- [27] R Brout, “Correlation energy of a high-density gas: Plasma coordinates,” *Phys. Rev.* **108**, 515–517 (1957).
- [28] T Ando, T Nakanishi, and R Saito, “Berry’s phase and absence of back scattering in carbon nanotubes,” *J. Phys. Soc. Jpn.* **67**, 2857–2862 (1998).
- [29] L I Magarill, A V Chaplik, and M V Éntin, “Spin-plasmon oscillations of the two-dimensional electron gas,” *JETP* **92**, 153–158 (2001).
- [30] A V Zayats, I I Smolyaninov, and A A Maradudin, “Nano-optics of surface plasmon polaritons,” *Phys. Rep.* **408**, 131–314 (2005).
- [31] A L Walter, A Bostwick, K-J Jeon, F Speck, M Ostler, T Seyller, L Moreschini, Y J Chang, M Polini, R Asgari, A H MacDonald, E Horn, and E Rotenberg, “Effective screening and the plasmaron bands in graphene,” *Phys. Rev. B* **84**, 085410 (2011).